Hindawi
Advances in Civil Engineering
Volume 2022, Article ID 5889743, 12 pages
https://doi.org/10.1155/2022/5889743

Research Article

Coupled CFD-FEM Simulation of Steel Box Bridge Exposed to Fire

Chenglong Xu[1] and Zhi Liu[2]

[1]*Guangzhou Expressway Co., Ltd., Guangzhou, China*
[2]*Department of Bridge and Tunnel Engineering, Southeast University, Nanjing 211100, China*

Correspondence should be addressed to Zhi Liu; mech.zhi@outlook.com

Received 26 May 2021; Revised 9 November 2021; Accepted 29 December 2021; Published 10 January 2022

Academic Editor: Vasant Matsagar

Copyright © 2022 Chenglong Xu and Zhi Liu. This is an open access article distributed under the Creative Commons Attribution License, which permits unrestricted use, distribution, and reproduction in any medium, provided the original work is properly cited.

Increasing fire-induced bridge failures are demanding more precise behavior prediction for the bridges subjected to fires. However, current numerical methods are limited to temperature curves prescribed for building structures, which can misestimate the fire impact significantly. This paper developed a framework coupling the computational dynamics (CFD) method and finite element method (FEM) to predict the performance of fire-exposed bridges. The fire combustion was simulated in CFD software, Fire Dynamic Simulator, to calculate the thermal boundary required by the thermomechanical simulation. Then, the adiabatic surface temperatures and heat transfer coefficient were applied to the FEM model of the entire bridge girder. A sequential coupled thermomechanical FEM simulation was then carried out to evaluate the performance of the fire-exposed bridge, thermally and structurally. The methodology was then validated through a real fire experiment on a steel beam. The fire performance of a simply supported steel box bridge was simulated using the proposed coupled CFD-FEM methodology. Numerical results show that the presented method was able to replicate the inhomogeneous thermomechanical response of box bridges exposed to real fires. The girder failed due to the buckling of a central diaphragm after the ignition of the investigated tanker fire in no more than 10 min. The framework presented in this study is programmatic and friendly to researchers and can be applied for the estimation of bridges in different fire conditions.

1. Introduction

Fire-induced damages to bridges appear as an increasing concern as more bridges failed due to vehicle fires [1–3]. The fire threat to bridges can be worse along with the prominent development of transport of inflammable products. By reducing the material strength dramatically, fires can result in partial or total collapses to bridges. Famous examples include MacArthur Maze, the I-65 overpass, and the more recent railway bridge in Tempe in the USA.

Exposed to fires, bridges deflect seriously and can reach the ultimate state at high temperatures. Even after fires, steel can also be degraded to a significant extent, as demonstrated in [4, 5]. General studies simplified the fire condition as the temperatures increased over time developed for building structures, such as the ISO834 [6] curve and ASTM119 fire [7], which belong to the layered temperature model developed for indoor fires [8]. Such investigations [9–11] to predict the fire performance of bridges are basically a thermomechanical finite element method (FEM) simulation by applying the simplified fire-induced surrounding temperature field to a hypothetical exposed structural portion. However, bridge fires usually have no air limitations. Adopting prescriptive temperature curves for fire-exposed bridges can underestimate surrounding temperatures and make the safety estimation unconvinced.

Comparatively, coupling the computational fluid dynamics (CFD) model of fire scenario and the FEM model of the exposed structural portion can provide a more realistic insight into the thermomechanical behavior of the bridges in fire conditions [12]. According to the CFD-FEM-based study [13] and experimental validation [14] on a simply supported bridge, this coupled approach can predict the structural behavior in a more complex but more precise way. Peris-Sayol et al. [15] adopted the coupled CFD-FEM method to analyze the behavior of a simply supported steel

bridge and analyze the parametric influence caused by horizontal constraint, modeled component count, vertical clearance, and wind. Increasing studies in recent years took the coupled CFD-FEM approach as an advanced tool to predict the performance of bridges in various fire conditions [16–18].

Despite that, the behavior of steel box girders in fire conditions has not been investigated by coupling CFD and FEM models. The fire-driven heat flow can be very complex confined to the crisscross plates of the main girder. Simplifying the fire environment as temperature curves can introduce significant deviations to the numerical prediction of the thermomechanical response of exposed bridges.

This paper presents a programmatic coupled CFD-FEM analysis for a steel box bridge subjected to a tanker fire that occurred beneath. The CFD model of the fire condition was developed in a fire dynamics platform, then the thermal boundary information was extracted, and lastly, the thermomechanical performance of the exposed bridge was analyzed through a sequentially coupled FEM simulation. Validated by experimental studies, this approach can be applied in future endeavors aiming at capturing a more precise fire response of bridges.

2. Methodology

Simulating the performance of a structure subjected to fire usually has three steps. The first step is to determine the temperature field surrounding exposed components. The second step is to perform a thermal analysis to obtain the inside temperature propagation. The last step is the structural simulation to evaluate the mechanical behavior. Due to the lack of data, previous studies [9, 11, 19] adopted the building-aimed temperature curves for bridges in the first step. Commonly used profiles included ISO834 [6] and ASTM119 [7] curves. This simplification can lead to obvious deviation to the bridge performance because the temperature curves designed for buildings underestimate the inhomogeneous thermal environment caused by bridge fires such as tanker fires usually have more intensive combustion processes than common indoor fires.

The CFD approach is an advanced tool to reproduce the fire scenario, providing a more accurate temperature distribution for following FEM simulations. One of the effective thriving CFD software is Fire Dynamics Simulator (FDS). It is a large-eddy simulation (LES) based code designed to model the fire-driven fluid flow by solving numerically the Navier–Stokes equations. The goal of the LES is to evolve the cell mean values of mass, momentum, and energy explicitly while accounting for the effects that subgrid transport and chemistry have on the mean fields. More mathematical models are demonstrated in [20].

Validated by various experiments, FDS is capable of predicting fire-related quantities, such as the gas-phase temperature field, heat flux, and smoke movement. FDS was thereby adopted in this study to reproduce the fire environment in the first step as described above. However, the general method of transferring heat fluxes from the fire model is very complex because numerous vector quantities are required. Wickström et al. [21, 22] proposed an easier method to transport the results from the fire model to the FEM model compared to using heat fluxes; that is, to assume a perfectly insulated surface overlaid on fire-exposed surfaces and calculate the heat flux using the hypothetical surface temperature, the adiabatic surface temperature, T_{AST}, and heat transfer coefficient, h:

$$\dot{q}''_{tot} = \varepsilon\sigma\left[\left(T_{\mathrm{AST}}\right)^4 - \left(T_{\mathrm{surf}}\right)^4\right] + h\left(T_{\mathrm{AST}} - T_{\mathrm{surf}}\right), \quad (1)$$

where ε is the surface emissivity, σ is the Stefan–Boltzmann constant, h is the convective heat transfer coefficient, and T_{surf} is the surface temperature. It shows that the heat fluxes imposed on surfaces can be determined by a single quantity T_{AST}, which can be measured using plate thermometers in experiments. Before the FDS simulation, measuring devices were arranged at the centroids of the elements adopted for discretizing these panels. The simulation process yields the T_{AST} and h in equation (1), providing the thermal boundary for following FEM calculations.

To determine the response of the exposed bridge, a sequentially coupled thermomechanical FEM simulation was carried out considering the thermal exposure extracted from the FDS process. The temperature field was calculated first and then was applied as the body load to the structural model transferred from the thermal model. Note that FDS can also calculate the surface temperature using the 1D heat transfer model neglecting the in-plane heat conduction. This can introduce a considerable inaccuracy compared with the real 3D thermal propagation. The presented coupled CFD-FEM methodology can consider the heat flow and the 3D thermal conduction and radiation more precisely. More details of the numerical framework can be found in [23].

3. Approach Validation

The experimental study carried out by Wickström et al. [24] was validated using the methodology presented in this paper. The tests were conducted inside a concrete chamber whose dimensions were 3.6 m× 2.4 m. Walls were 0.2 m thick, and their emissivity was taken as 0.8 [8]. Below the beam, there was a 0.3 m × 0.3 m burner releasing a constant 450 kW propane fire whose surface was 0.65 m over the floor. There were three tests in total. This paper performed a coupled CFD-FEM simulation for the specimen in Test 3, whose configuration is shown in Figure 1. The specimen was a steel I-beam hanging beneath the ceiling. The height and width of the specimen section were both 200 mm, and the thicknesses of the web and flanges were 9 mm and 15 mm respectively. The distance between the bottom flange and the floor was 2 m.

To capture the response of the specimen beam, three measuring stations, namely, A, B, and C, were arranged along the longitudinal axis. Quick-tip thermocouples were adopted to measure the temperatures of surfaces. The density of concrete walls was $600 \pm 100\,\mathrm{kg/m^3}$, and the specific heat and the conductivity were 800 J/kgK and 0.1 W/mK, respectively.

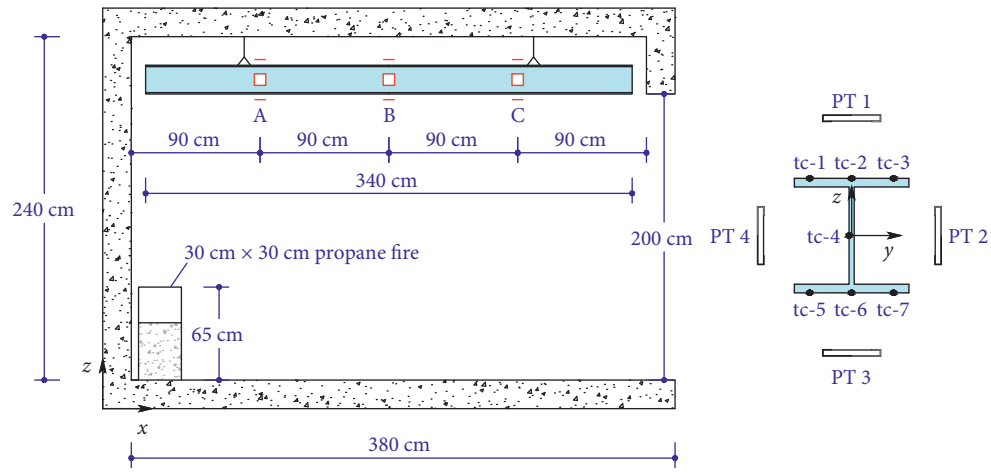

Figure 1: Configuration of Test 3 conducted by Wickström et al. [24].

The FDS fire model was developed considering the specimen and the chamber. The temperature-dependent material properties were considered according to Eurocode [25], and the fraction of fuel mass converted into smoke particulate was taken as 0.015 [24]. The dimensions of the computational domain were 4.4 m, 2.8 m, and 2.6 m in x, y, and z directions, respectively. There were 256,256 cubic cells in total whose side length was 5 cm.

Figure 2 compares the measured and calculated surface temperatures. The experimental and numerical results had a fine agreement with maximum differences of 5.3%, 3.2%, and 1.8% at three measuring stations, respectively. The measured temperatures were slightly lower than simulated results mainly due to the unidentical material models of the real specimen and that adopted in the coupled CFD-FEM simulation. Note that although this experiment was carried out inside a concrete chamber, the validation is still effective for open-fire scenarios in bridges because the crux of the CFD-FEM method is the coupling procedure instead of the boundary condition.

Overall, the simulated response of the specimen agrees well with the real fire scenario. Thereby, the presented coupled CFD-FEM approach was experimentally validated and was adopted to analyze the performance of fire-exposed bridges.

4. Engineering Background

4.1. Prototype Bridge. The investigated prototype bridge is shown in Figure 3. It is a steel box beam bridge simply supported with a span of 66.65 m and a length of 67.85 m. The bridge is symmetrical both longitudinally and laterally. It spans a two-way six-lane highway with a clearance of 8.911 m from the deck bottom to highway pavement. The cross-section of the bridge girder has two hollow thin-walled boxes, each of which is composed of one 2.3-m-wide floor, two 3.32-m-high webs, and 6 longitudinal stiffeners. In the lateral direction, the girder boxes are jointed through four types of diaphragms, namely, S, C, T, and D, which are shown in Figure 3(b). The composed deck is 10.8 m wide and 3.32 m deep. In the longitudinal direction, the roof is 18 or 20 or 30 mm thick, the floor is 30 or 35 or 40 mm thick, and the web is 16 or 18 mm thick. All of these panels and stiffeners are made of Q345 steel. On each end, the deck is supported by a twin-limb pier through two bearings.

4.2. Fire Scenario and Loading Condition. Surrounding the prototype bridge, numerous plants are producing inflammable chemicals. Potential fires can be triggered by the frequent transport of these products. This study considered a tanker fire that occurred beneath the bridge. The fire source was assumed as 2.8 m (x) × 8 m (y) × 2 m (z) in dimensions, locating centrally in the longitudinal axis and 2 m east of the longitudinal-vertical symmetry plane. The fire surface was 6.9 m below the girder bottom surface.

Spontaneous fire combustion usually contains three stages, which are the growth stage, steady stage, and decay stage. The heat release rate per unit area (HRRPUA) can be adopted to quantify the fire intensity. Existing studies on fire impacts to bridges [9, 14, 26–28] evaluated the HRRPUA ranging from 1600 to 3290 kW/m^2. This study considered an HRRPUA of 2400 kW/m^2. The maximum heat release rate (HRR) of the tanker fire was 53.76 MW. The fire was assumed to sustain 60 min until it was extinguished by fire-fighting forces.

When the bridge is exposed to fire, the combustion soot will be notable and the vehicles in the vicinity will dodge. If there are sporadic cars on the bridge, the load can also be neglected due to the less importance of the living load, which has been demonstrated in [9, 26]. Thereby only the gravity of the main girder and bridge facilities was considered.

5. Fire-Thermomechanical Response

5.1. Fire Behavior. The combustion process considering the gas flow influenced by obstructions was simulated by developing an FDS fire model as shown in Figure 4. The computational space, in which the simulation was carried out, was defined as 74.4 m (x) × 16 m (y) × 18 m (z). The domain was discretized by 2,678,400 cubic cells with a grid interval of 0.2 m, which was determined by the user manual

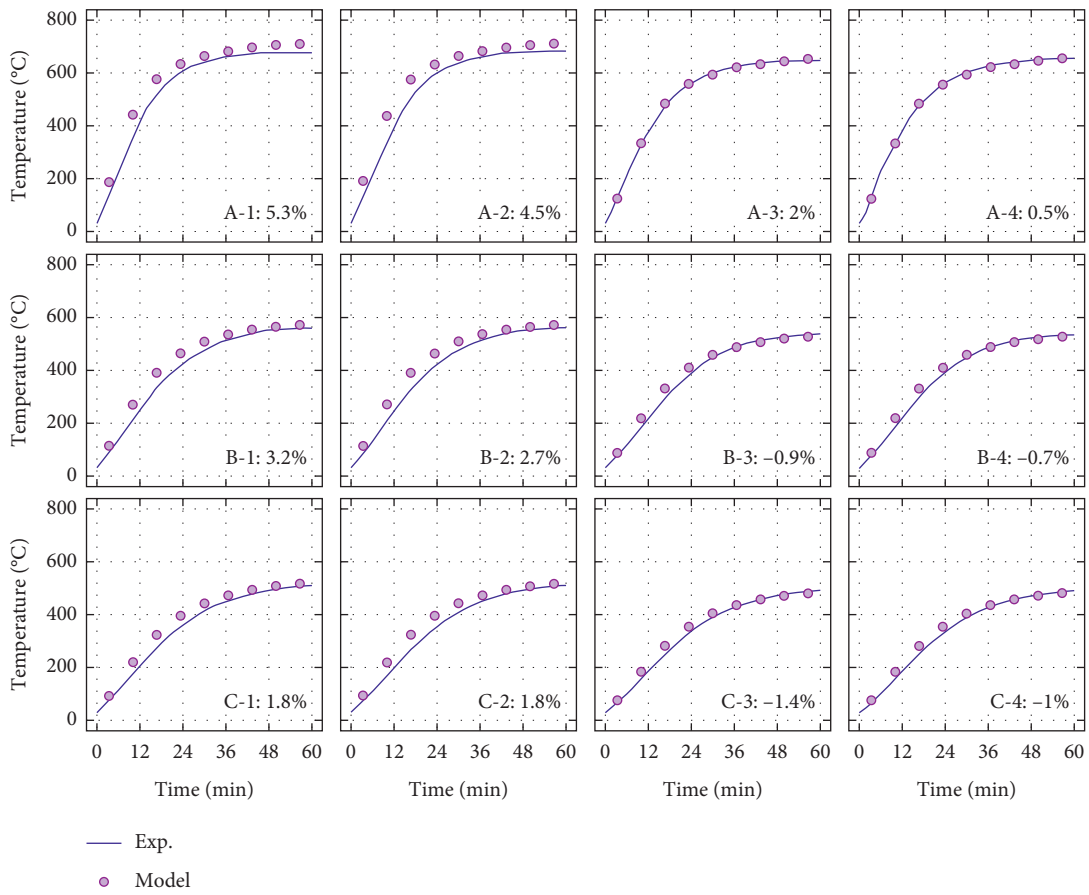

Figure 2: Comparisons between measured and calculated surface temperatures.

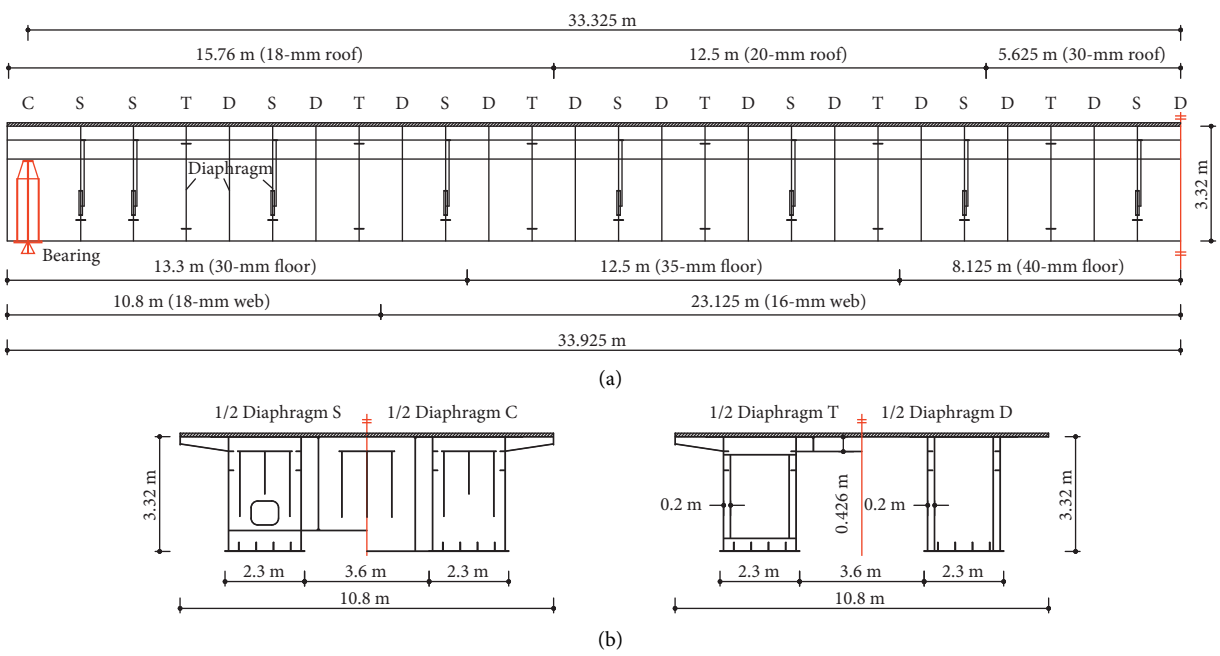

Figure 3: Structural profile of bridge girder: (a) elevation view of main plates; (b) section view of diaphragms S, C, T, and D.

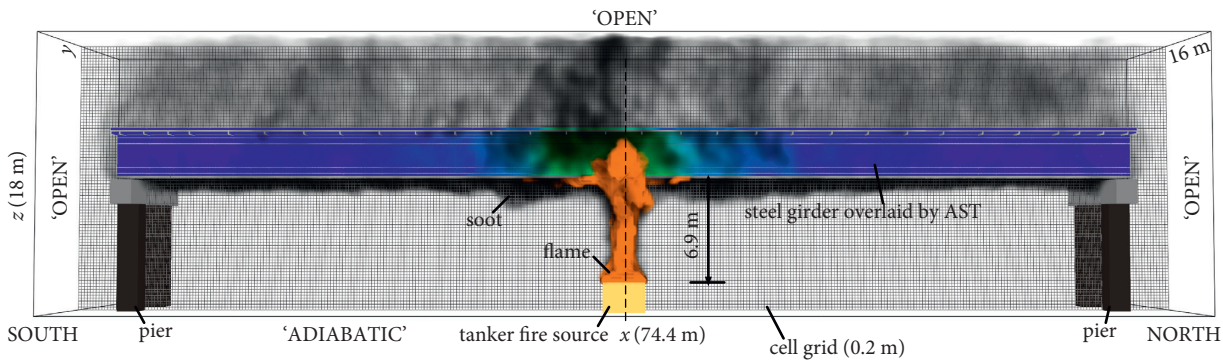

Figure 4: FDS model and fire behavior.

of FDS [29] and the report by the U.S. Nuclear Regulatory Commission [30]. Concrete piers were modeled as solid obstructions and steel girders were considered as thin-walled panels assigned with thermal material property varying with temperatures as specified in Europe standard [25]. The bottom edge of the computational domain was modeled as a concrete floor whose temperature remained constant at 20°C, and other space edges were passively opened to the surrounding environment. The open boundary is where fluid is allowed to flow into or out of the computational domain depending on the local pressure gradient. The boundary condition for the pressure depends on whether the local flow is incoming or outgoing.

The fire behavior and an overview of T_{AST} are presented in Figure 4. The 53.76 MW fire source engendered a flame reaching the girder floor. Due to the 2 m eastern deviation of the fire, the flame engulfed the east box of the girder. In Figure 4, the geometry of the bridge deck is overlaid by the transient T_{AST}, and the results of piers and cap beams were not recorded to save the time cost in the extracting process for boundary results. The flame geometry and T_{AST} distribution oscillated drastically due to the fire-driven plume and remained at a dynamic steady state after the fire became stable.

Figures 5 and 6 present the time-averaged gas temperature from the elevation ($y = 2$ m) and sectional view ($x = 0$), respectively. The intercepted elevation plane was inside the east girder box. It is shown that the temperature of the gas inside the central three enclosures was also increased significantly. Due to the upward fire-driven flow, the gas temperature in the vicinity of the midspan is very inhomogeneous. This verified that the layered temperature model built for indoor fires [8] is not suitable for box bridges. The maximum gas temperature was around 1060°C at the bottom surface of the east box above the fire. Note that the peak temperatures in the two views were slightly different due to the spatial-averaged calculation algorithm. In the lateral direction, a portion of the hot gas flowed out of the space enclosed by the roof and two central webs, introducing exposure to the east flange. The gas in the east box had a higher temperature than that in the west box. The inside temperature elevation was attributed to the radiation from the hotter webs and floors.

5.2. Thermal Response. To find the fire-induced performance of the bridge girder, the thermomechanical FEM model was developed in the ANSYS platform based on the designed profiles as shown in Figure 3. Main structural panels in the bridge girder were considered, including roofs, floors, diaphragms, webs, and longitudinal stiffeners. The uniform element size of 0.6 m was used to discretize all plates. The heat transfer including convection and radiation was analyzed using the 3-dimensional layered element type SHELL131 with in-plane and through-thickness thermal conduction capability. On both sides of each SHELL131 element, surface effect elements (SURF152) were overlaid to consider the effect of both radiation and convection between exposed surfaces and their proximities. The developed FEM model had 25,520 shell elements and 51,040 surface elements in total.

Steel is very sensitive to temperatures [31] that its thermal and mechanical properties can change significantly at high temperatures. The temperature-dependent material property in Eurocode [25] shown in Figure 7 was adopted for the deck steel because its applicability has been validated by numerous experimental and numerical studies [13, 14, 28, 31]. Around 750°C, the thermal expansion remains constant because of the austenitization-induced counteraction. The adiabatic surface temperature, T_{AST}, and heat transfer coefficient, h, calculated by the FDS simulation was applied as the boundary of the thermal FEM model and were assigned to the extra nodes and applied on the surface elements, respectively. To determine the fire-induced response of the girder, a sequential coupled thermomechanical simulation was performed. The 60 min thermal simulation was carried out considering a maximum and minimum time step of 1 s and 10 s, respectively. The Newton–Raphson solution method is applied to reach convergence at each iteration within a time step, and nonlinearities of material and geometry were considered. However, the structural simulation did not converge at 535 s using the minimum time step of 0.005 s.

Figure 8 shows the temperature distribution of main plates at the failure moment. The portion over the fire source was remarkably affected in its temperature and the parts on two ends were not thermally influenced. Because of the isolation of floors, the temperature of the roof in two girder boxes was mainly affected by radiation and was not

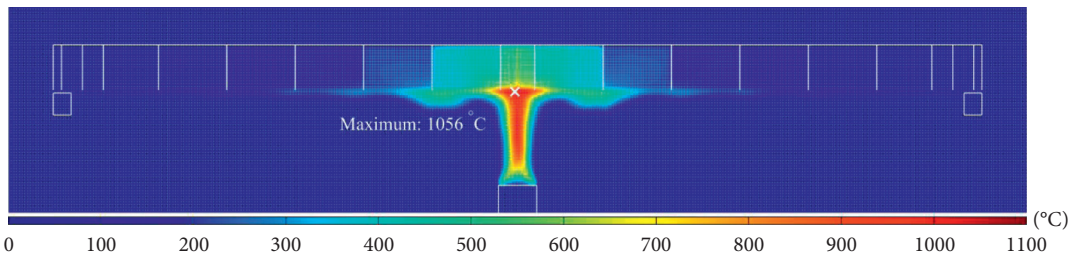

Figure 5: Gas temperature (elevation view).

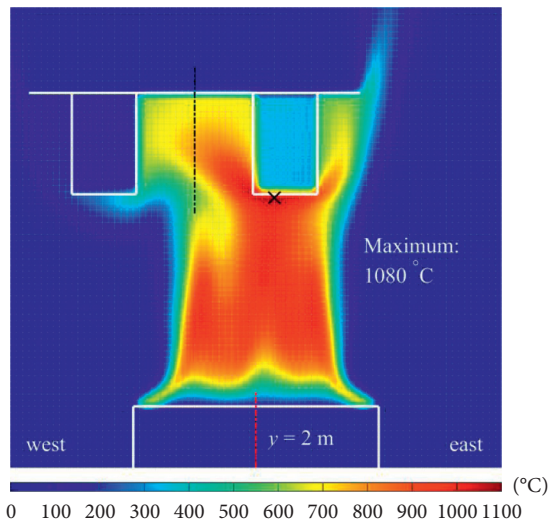

Figure 6: Gas temperature (sectional view).

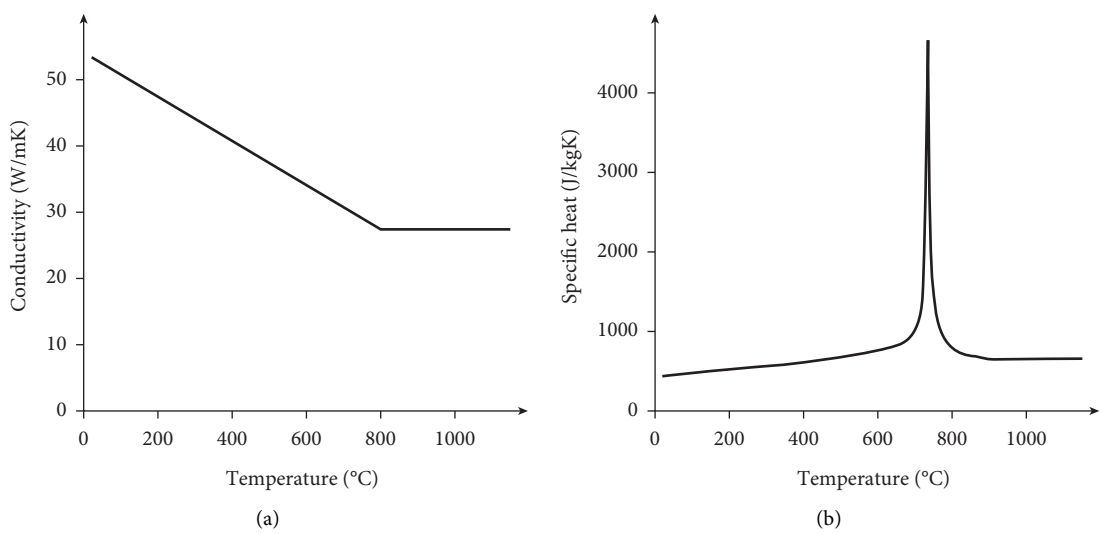

Figure 7: Continued.

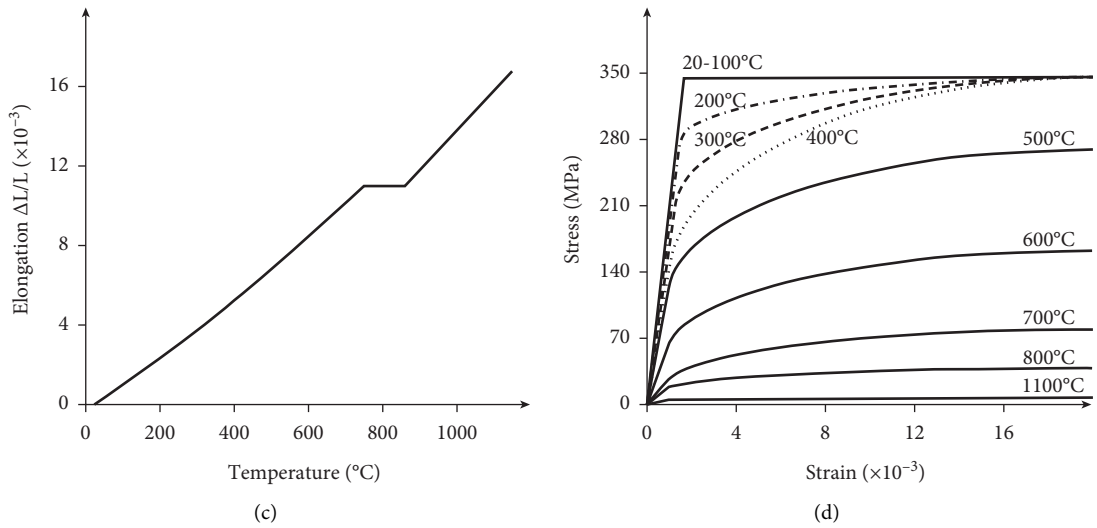

Figure 7: Material property of deck steel: (a) conductivity; (b) specific heat; (c) elongation; and (d) stress–strain relationship.

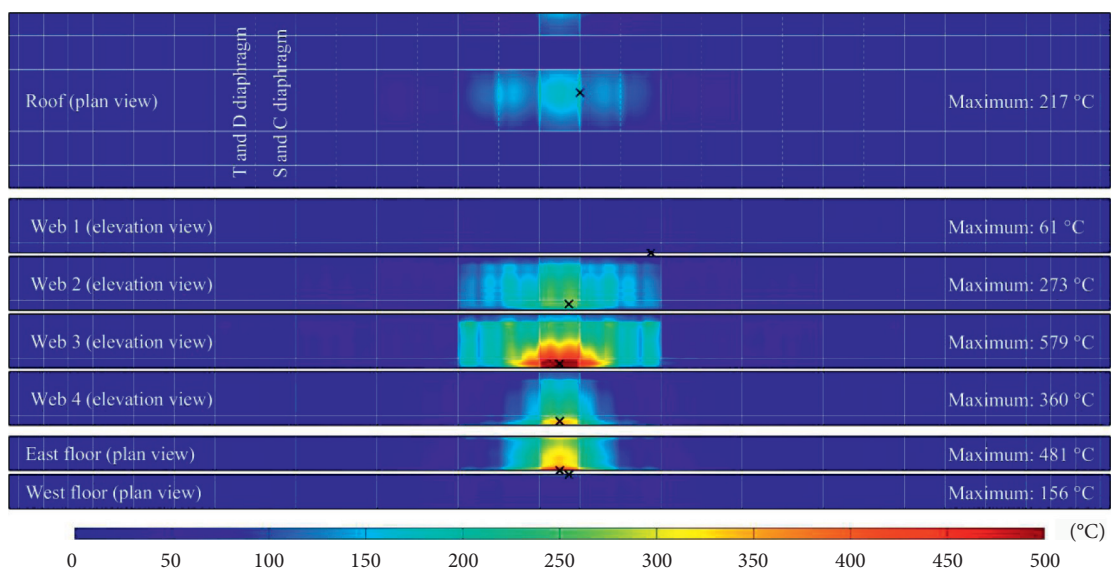

Figure 8: Isotherm of main plates at failure.

increased obviously. However, the temperature of the central roof was dramatically elevated because it was directly exposed to the fire. The lateral deviation of the fire source enhanced the temperature of the east flange compared to the west flange. In each box, two webs were contained. The four webs in the girder we denoted as web 1 to web 4 from west to east. The westmost web was almost unaffected by the tanker fire because the flame was confined to the domain enclosed by two central webs. Exposed directly to the flame, the west web of the east box had the most significant temperature increment in its bottom part up to 579°C. The temperature at the central portion of the eastmost and west webs was also raised by around 360°C due to conduction and convection. Compared to web 4, web 2 had a broader influenced district because the former was directly exposed to flame and the heat flow overflowed whereas the latter was heated by the hot gas gathered in the enclosures between two central webs. Regarding the floor, the east one also received the most exposure and had a higher temperature up to 481°C. The temperature of the west floor was not obviously affected by the fire source.

Figure 9 shows the isotherm for the central two S-type diaphragms, which were 1.25 m and 6.25 m far from the bridge centerline, respectively. The closest S-type diaphragm was increased in its temperature up to 694°C in the east part that was over the fire source and the temperature of the west portion was also elevated significantly by the enclosed hot gas. In the further diaphragm that is 6.25 m away from the bridge centerline, the temperature was increased up to 91°C because the generated heat flow engulfed the girder bottom.

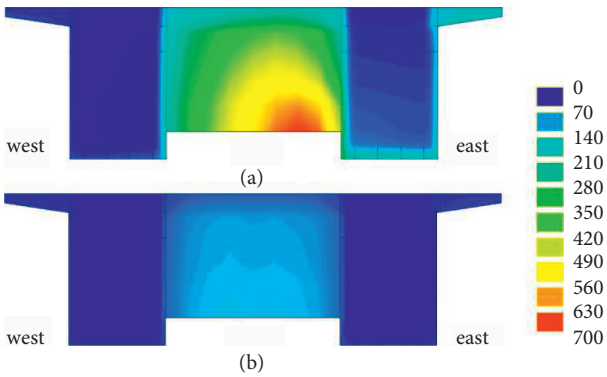

Figure 9: Isotherm of S-type diaphragms at failure: (a) diaphragm 1.25 m from bridge centerline; and (b) diaphragm 6.25 m from bridge centerline (unit: °C).

Comparatively, the temperature of the portion in the two boxes was not increased notably because no direct fire exposure was imposed although the gas temperature was increased as shown in Figure 6.

5.3. Structural Response. The developed structural FEM model was obtained based on the thermal FEM model described above by removing surface effect elements and transferring the element type from thermal element to structural element. The structural model had the same discretization as the thermal FEM model as shown in Figure 10. In the north end of the bridge, the deck bottom was constrained in its vertical and longitudinal directions, and only the vertical degrees of freedom were restricted at the south end. The constrained locations were these nodes of the girder floor supported by bearings [32]. To ensure the structural determination in the lateral direction, one node at the north bearing was laterally constrained. The spatially and temporally resolved temperature response was applied to the structural FEM model as body loads for the structural simulation. The mechanical property of deck material at high temperatures was adopted from the Eurocode [25] as shown in Figure 7.

Figure 11 shows the stress distribution for the main plates of the girder at failure. The fire source increased the stress in a considerable portion of the girder. The high-stress district is the plates enclosing central seven chambers, including the roof and two central webs. The stress in the roof was increased significantly up to 227 MPa. The two central webs, web 2 and 3, were directly exposed to heat flows and had higher stresses at the districts connecting other plates, reaching up to 262 MPa and 236 MPa, respectively. The other two side webs had a lower stress elevation mainly due to the expansion of neighboring panels. Regarding the floor, the stress at the welding district of the inner east floor edge and the closest diaphragm to fire was elevated to 202 MPa. Comparatively, the east floor had a global stress elevation up to over 100 MPa. The difference in the stress enhancement of the girder floor was mainly because the east floor is influenced partially by the fire whereas the stress in the west floor is interpreted as the fire-induced response of the global girder.

Figure 12 presents the stress distribution of the two S-type diaphragms 1.25 m and 6.25 m far from the bridge centerline, respectively. The closest S-type diaphragm had the highest stress at 320 MPa in its inner side at the bottom of the east box. Referring to the isotherm displayed in Figure 9(a), the locations with the maximum temperature had a comparatively lower stress level instead of the maximum stress. This is because the ultimate stress of material at high temperatures has been reduced to a value much lower than that at ambient temperature. The stress of the diaphragm 6.25 m far away from the bridge centerline had more uniform stress as it is less influenced by the localized fire.

Figure 13 shows the deformation of the roof, including five longitudinal paths and one lateral path. The longitudinal paths included the longitudinal roof centerline and the top edges of four webs, and the lateral path is the lateral roof centerline. Note that the shape only represents the fire-induced deformation. Due to the fire-induced high temperature, the centerline of the girder roof deformed up to 9.0 mm downward and 1.8 mm upward. The wavy configuration was mainly caused by the thermal expansion obstructed by diaphragms, as shown by the vertical lines in Figure 13.

In each box, the two webs had a close deformation. The two boxes deformed by around 4.0 mm and 4.6 mm, respectively. This means the two boxes behaved separately and integrally under the eccentric fire load due to the considerable bending and torsional stiffnesses of the box configuration. Because the fire source deviated to the east, the east box was exposed to more heat and deformed more significantly. The sectional view shows that the global girder deformed and rotated towards the fire due to the eccentric temperature propagation. Through the calculation based on the top edges of the central two webs, the section rotated 0.1163° subjected to the eastern deviated tanker fire.

International standards have some specifications on defining the failure criteria of fire-exposed beam structures. For instance, BS 476–10 : 2009 stipulates a vertical deformation of $L/20$ and a limiting rate of deflection of $L^2/9000d$ over 1 min, which means a beam subjected to fire can be considered as failed when any of the two indicators is reached. However, none of these specified criteria was satisfied in this studied case at the moment that the FEM simulation did not converge at 535 s. These prescriptive criteria are usually applicable when simulations can converge or experimental specimens can survive, leaving a decision space for engineers. In this case, the bridge can only sustain 535 s in the investigated 53.76-MW tanker fire.

The failure model is displayed in Figure 14 with the roof being hidden. It is shown that the girder failed due to the out-of-plane buckling of the diaphragm closest to the fire source. Figures 8 and9 show that the closest diaphragms had the highest response at 694°C, which is significantly higher than the temperature of main panels, which peaked at 579°C. This is because diaphragms received two-side exposures, whereas other panels were exposed to hot gases only on one side. Subjected to the serious expansion confined by central two webs, the diaphragms closest to the fire buckled out of the plane.

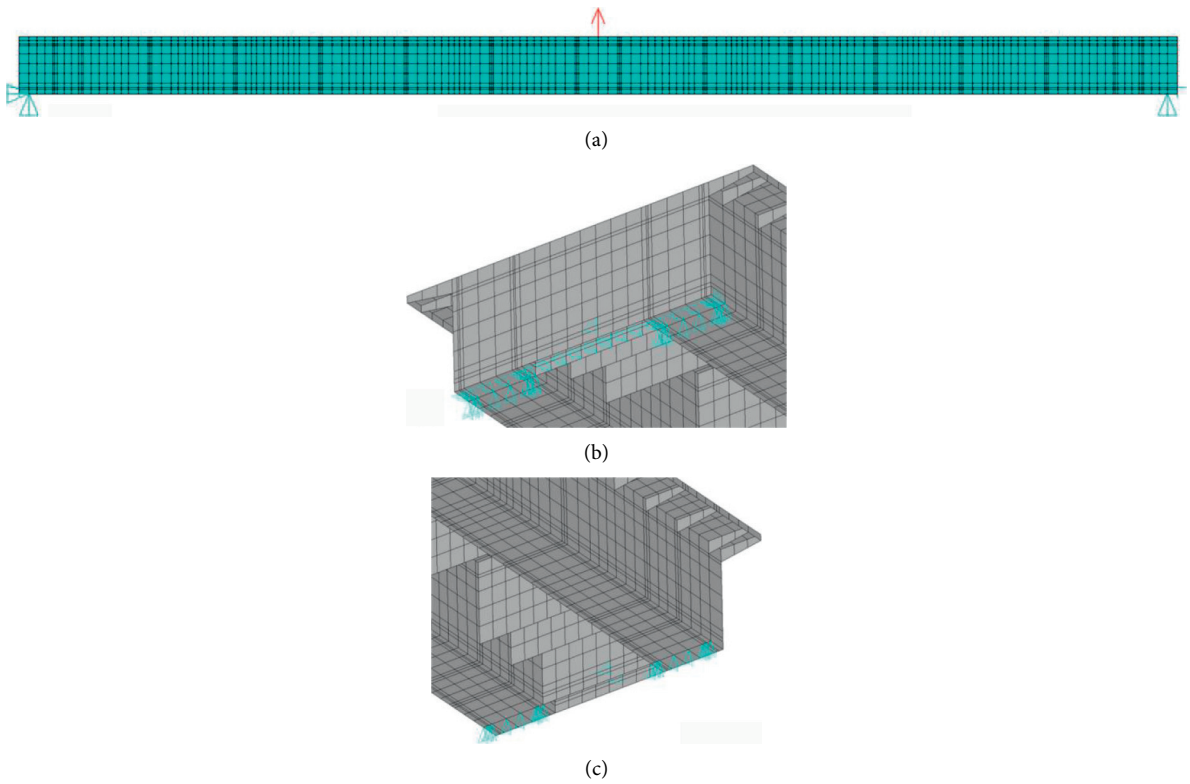

Figure 10: Structural FEM model of bridge girder: (a) elevation view; (b) north bearing; and (c) south bearing.

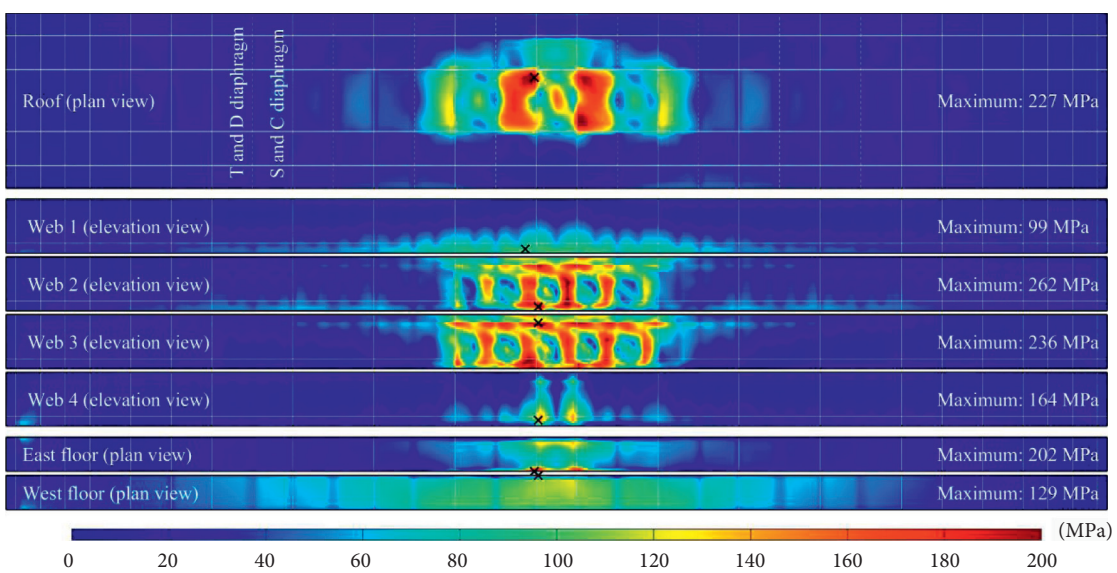

Figure 11: Mises stress of main plates at failure.

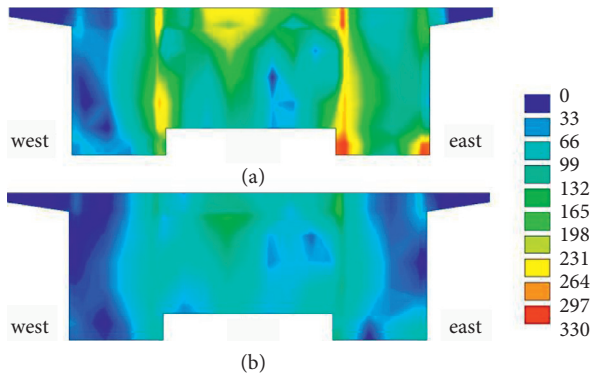

Figure 12: Stress distribution of S-type diaphragms at failure: (a) diaphragm 1.25 m from bridge centerline and (b) diaphragm 6.25 m from bridge centerline (unit: MPa).

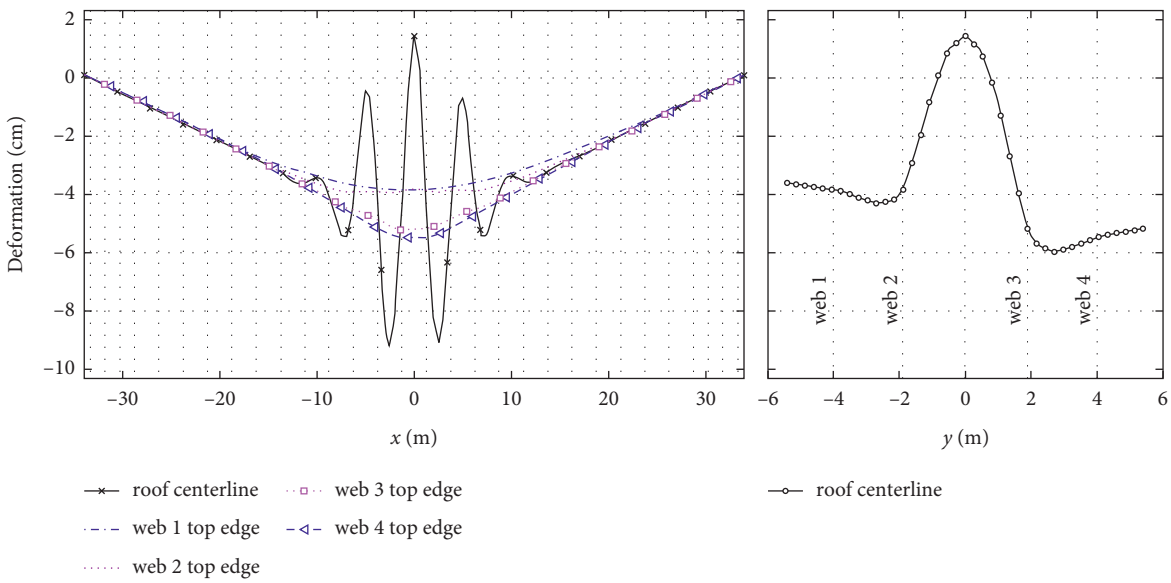

Figure 13: Roof deformation at failure.

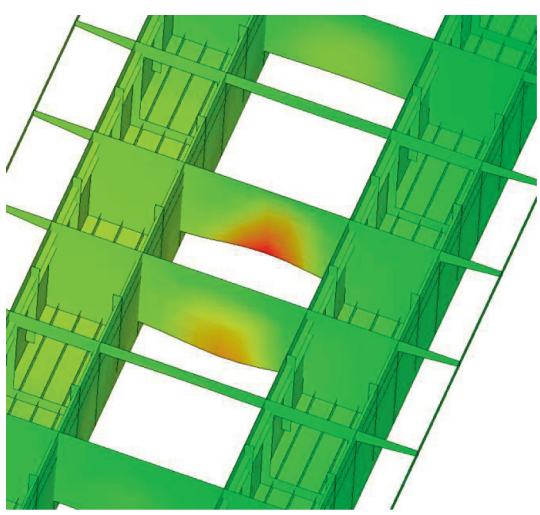

Figure 14: Failure model of girder (the roof is hidden).

6. Conclusion

This paper presents a coupled CFD-FEM approach for numerically predicting the behavior of fire-exposed box bridges. The fire-driven flow was simulated adopting the CFD model, and the thermomechanical behavior was captured using a FEM model. This methodology was validated based on a real fire experiment on a steel beam with a good agreement resultant.

Then a steel box bridge with a tanker fire beneath was investigated based on the coupled CFD-FEM approach. The hypothetical tanker fire with a maximum power of 53.76 MW that occurred at midspan introduced a dramatic impact on the bridge. The temperatures of exposed panels, especially diaphragms and welding portions between webs, floors, and diaphragms, were increased significantly. As a result, a considerable portion of plates was elevated in their stress. The 2 m lateral eastern deviation of the fire source forced the girder to deform and rotate towards the fire source. The girder failed after less than 10 min due to the out-of-plane buckling of the central diaphragm.

Compared to existing works, this study introduced a programmatic framework to transfer the boundary information from the CFD-based fire model to the thermomechanical FEM model, avoiding adopting less accurate temperature curves simplifying the fire environment as spatially uniform temperature distribution. The fire-induced gradient thermomechanical response of the bridge girder was reproduced by using the coupled CFD-FEM simulation. The presented study was carried out using a programmatic process and can be extended to other bridges in fire conditions.

Data Availability

All data, models, or codes that support the findings of this study are available from the corresponding author upon reasonable request.

Conflicts of Interest

The authors declare that they have no conflicts of interest.

References

[1] I. E. Harik, A. M. Shaaban, H. Gesund, G. Y. S. Valli, and S. T. Wang, "United States bridge failures, 1951-1988," *Journal of Performance of Constructed Facilities*, vol. 4, no. 4, pp. 272–277, 1990.

[2] K. Wardhana and F. C. Hadipriono, "Analysis of recent bridge failures in the United States," *Journal of Performance of Constructed Facilities*, vol. 17, no. 3, pp. 144–150, 2003.

[3] M. Garlock, I. Paya-Zaforteza, V. Kodur, and L. Gu, "Fire hazard in bridges: review, assessment and repair strategies," *Engineering Structures*, vol. 35, pp. 89–98, 2012.

[4] T. Molkens, K. A. Cashell, and B. Rossi, "Post-fire mechanical properties of carbon steel and safety factors for the reinstatement of steel structures," *Engineering Structures*, vol. 234, Article ID 111975, 2021.

[5] E. Aziz and V. Kodur, "An approach for evaluating the residual strength of fire exposed bridge girders," *Journal of Constructional Steel Research*, vol. 88, pp. 34–42, 2013.

[6] ISO, *Fire Resistance Tests - Elements of Building Construction*, ISO, Geneva, Switzerland, 1975.

[7] 2001 Materials ASfTa. ASTM E119: Standard Test Methods for Fire Tests of Building Construction and Materials.

[8] 2002 CEN. Eurocode 1: Actions on structures - Part 1-2: General actions Actions on structures exposed to fire.

[9] I. Payá-Zaforteza and M. E. M. Garlock, "A numerical investigation on the fire response of a steel girder bridge," *Journal of Constructional Steel Research*, vol. 75, pp. 93–103, 2012.

[10] S.-H. Yun and J.-S. Jeon, "Post-fire damage assessment of Korean bridges using thermal–structure interaction fire analysis," *Magazine of Concrete Research, ICE*, vol. 70, pp. 938–953, 2017.

[11] G. Zhang, V. Kodur, C. Song, S. He, and Q. Huang, "A numerical model for evaluating fire performance of composite box bridge girders," *Journal of Constructional Steel Research*, vol. 165, pp. 1–10, 2020.

[12] J. Choi, *Concurrent Fire Dynamics Models and Thermomechanical Analysis of Steel and concrete Structures*, Georgia Institute of Technology, Atlanta, Georgia, 2008.

[13] J. Alos-Moya, I. Paya-Zaforteza, A. Hospitaler, and E. Loma-Ossorio, "Valencia bridge fire tests: validation of simplified and advanced numerical approaches to model bridge fire scenarios," *Advances in Engineering Software*, vol. 128, pp. 55–68, 2019.

[14] J. Alos-Moya, I. Paya-Zaforteza, A. Hospitaler, and P. Rinaudo, "Valencia bridge fire tests: experimental study of a composite bridge under fire," *Journal of Constructional Steel Research*, vol. 138, pp. 538–554, 2017.

[15] G. Peris-Sayol, I. Paya-Zaforteza, J. Alos-Moya, and A. Hospitaler, "Analysis of the influence of geometric, modeling and environmental parameters on the fire response of steel bridges subjected to realistic fire scenarios," *Computers & Structures*, vol. 158, pp. 333–345, 2015.

[16] Q. Zou, K. Pool, and S. Chen, "Performance of suspension bridge hangers exposed to hazardous material fires considering wind effects," *Advances in Bridge Engineering*, vol. 1, 2020.

[17] X.-Q. Wu, T. Huang, F. T. K. Au, and J. Li, "A localized fire model for predicting the surface temperature of box girder bridges subjected to tanker truck fire," *Fire Technology*, vol. 56, 2020.

[18] R. Ma, C. Cui, M. Ma, and A. Chen, "Numerical simulation and simplified model of vehicle-induced bridge deck fire in the full-open environment considering wind effect," *Structure and Infrastructure Engineering*, vol. 17, no. 12, pp. 1698–1709, 2020.

[19] E. M. Aziz, V. K. Kodur, J. D. Glassman, and M. E. Moreyra Garlock, "Behavior of steel bridge girders under fire conditions," *Journal of Constructional Steel Research*, vol. 106, pp. 11–22, 2015.

[20] K. McGrattan, S. Hostikka, J. Floyd, R. McDermott, and M. Vanella, "Fire dynamics simulator technical reference guide," *Mathematical Modelling*, vol. 1, 2019.

[21] U. Wickström, A. Robbins, and G. Baker, "The use of adiabatic surface temperature to design structures for fire exposure," *Journal of Structural Fire Engineering*, vol. 2, pp. 21–28, 2011.

[22] U. Wickström, D. Duthinh, and K. B. McGrattan, "Adiabatic surface temperature for calculating heat transfer to fire

exposed structures," in *Proceedings of the Eleventh International Interflam Conference Interscience Communications*, London, USA, 2007.

[23] Z. Liu, J. C. G. Silva, Q. Huang, Y. Hasemi, Y. Huang, and Z. Guo, "Coupled CFD–FEM simulation methodology for fire-exposed bridges," *Journal of Bridge Engineering, ASCE*, vol. 26, 2021.

[24] U. Wickström, R. Jansson, and H. Tuovinen, *Validation Fire Tests on Using the Adiabatic Surface Temperature for Predicting Heat Transfer*, SP Technical Research Institute of Sweden, Borås, Sweden, 2009.

[25] C. EN. Eurocode 3, *Design of Steel Structures - Part 1-2: General Rules Structural Fire Design*, European Committee for Standardisation, Brussels, Belgium, 2005.

[26] J. Alos-Moya, I. Paya-Zaforteza, M. E. M. Garlock, and E. Loma-Ossorio, "Analysis of a bridge failure due to fire using computational fluid dynamics and finite element models," *Engineering Structures*, vol. 68, pp. 96–110, 2014.

[27] X. Gong and A. K. Agrawal, "Numerical simulation of fire damage to a long-span truss bridge," *Journal of Bridge Engineering, ASCE*, vol. 20, 2015.

[28] X. Gong and A. K. Agrawal, "Safety of cable-supported bridges during fire hazards," *Journal of Bridge Engineering, ASCE*, vol. 21, no. 4, Article ID 04015082, 2016.

[29] K. McGrattan, S. Hostikka, J. Floyd, R. McDermott, and M. Vanella, *Fire Dynamics Simulator User's Guide*, US Department of Commerce, Washington, D.C., United States, 2019.

[30] A. P. Hamins and K. B. McGrattan, *Verification and Validation of Selected Fire Models for Nuclear Power Plant Applications*, U.S. Nuclear Regulatory Commission, Rockville, Maryland, United States, 2007.

[31] J. M. Atienza and M. Elices, "Behavior of prestressing steels after a simulated fire: fire-induced damages," *Construction and Building Materials*, vol. 23, pp. 2932–2940, 2009.

[32] D. Pantusoa, K.-J. Bathea, and P. A. Bouzinovb, "A finite element procedure for the analysis of thermomechanical solids in contact," *CoStr*, vol. 75, pp. 551–573, 2000.